Photocatalytic facile ZnO nanostructures for the elimination of the antibiotic sulfamethoxazole in water

Photocatalytic facile ZnO nanostructures for the elimination of the antibiotic sulfamethoxazole in water

Tatiana Makropoulou[a], Ioannis Kortidis[b], Konstantina Davididou[a], David E. Motaung[b,c], Efthalia Chatzisymeon[a,*]

[a]School of Engineering, Institute for Infrastructure and Environment, University of Edinburgh, The King's Buildings, Edinburgh EH9 3JL, United Kingdom

[b]DST/CSIR National Centre for Nanostructured Materials, Council for Scientific and Industrial Research, Pretoria 0001, South Africa

[c]Department of Physics, University of the Free State, P.O. Box 339, Bloemfontein ZA9300, South Africa

*Corresponding Author: e.chatzisymeon@ed.ac.uk; 0044(0)1316505711

Abstract

The degradation of sulfamethoxazole (SMX) by a synthesized ZnO catalyst and under UVA irradiation was examined. ZnO nanostructures were developed by a facile hydrothermal-assisted method. The effect of ZnO heating time and synthesis reaction, pH, catalyst loading, and SMX initial concentration on process efficiency was studied. Water matrices, such as humic acid (HA) solution and surface water (SW), were also used to resemble real environmental water samples. It was observed that when ZnO is synthesized at pH 7.5, nanorods grow on its surface, while nanoplatelets are formed when synthesis takes place at pH 12.5. SMX removal reached 84% after 60 min of treatment in the presence of 200 mg/L ZnO catalyst (8 h-heated at pH 7.5; C_0 = 10 mg/L). The pseudo-first-order kinetic constants of SMX photodegradation were calculated at 0.039, 0.030 and 0.016 min^{-1} for 5, 10, and 20 mg/L SMX, respectively. This decreased efficiency was attributed to the excessive coverage of catalyst surface by SMX molecules, evidenced by SEM micrographs produced after treatment. SMX degradation in SW (12.5%) was considerably lower than in UPW (47.4%) due to the presence of natural organic matter in the first. Interestingly, SMX removal was greatly enhanced in HA matrix (99%) and this can be attributed to the ability of HA to sensitize colloidal ZnO. In all cases, morphological changes of ZnO nanostructures were observed after photocatalytic treatment. It was confirmed that SMX degradation takes place through $HO^{\bullet}$ by adding $HO^{\bullet}$ quenchers, such as *tert*-butyl alcohol and methanol, in the reactant mixture.

Keywords: wastewater treatment; pharmaceuticals; priority pollutants; Advanced oxidation; semiconductors; heterogeneous photocatalysis

1. Introduction

Antibiotics are vital for safeguarding human health and have saved millions of lives over the years since their first discovery. Nonetheless, current research indicates that overuse is making antibiotics less effective, since bacteria mutate and develop resistance to them. Antibiotic resistant bacteria (ARB) are developed by mutations emerged from prolonged exposure nullifying antibiotic defense against bacterial infections (Lupo and Coyne, 2012). Therefore, as people continue to overuse antibiotics, as well as over-expose livestock animals to control possible infections, resistant bacteria not only survive but instead thrive. ARB can be found in numerous environments, such as hospitals, waters or crops and are a great challenge in infectious diseases today (Jiang et al., 2013; Giannakis et al., 2018). Each year, ARB infections lead to 700,000 deaths globally, while healthcare costs are expected to rise up to 2.9 trillion USD by 2050 (OECD, 2016). In addition to the development of ARB, the growing use of antibiotics, exacerbated by their xenobiotic nature, has increased contamination of natural waters and bioaccumulation risk in the food chain (Lupo and Coyne, 2012). For example, sulfamethoxazole (SMX), which is a sulfonamide antibiotic has been widely detected in wastewater treatment plant (WWTP) effluents, surface and drinking water bodies (Fatta-Kassinos et al., 2011; Ribeiro et al., 2016; Lee et al., 2019). SMX is extensively prescribed to treat infectious and respiration diseases in human and veterinary medicine and to promote animal growth (Xekoukoulotakis et al., 2011; Mirzaei et al., 2018b).

Currently, when antibiotics enter conventional biological WWTPs, only a small fraction of them is removed (Karaolia et al., 2018). This is due to the fact that existing WWTPs were not originally designed to cope with such persistent contaminants (Fatta-Kassinos et al., 2011; Barbosa et al., 2016). As a result, antibiotics are released into the terrestrial and aquatic

environment through disposal or water reuse applications, causing major environmental and health concerns (Martin-Laurent et al., 2019). Finding an effective technology to treat antibiotics in the environment is a major scientific challenge, which has received attention only the last decade.

Heterogeneous photocatalysis is an advanced oxidation process (AOP) that can effectively degrade recalcitrant compounds (Byrne et al., 2018; Lee et al., 2019; Lin and Wu, 2019). In principle, irradiation of photocatalysts like ZnO with photons having equal or higher energy level than catalysts' band gap triggers the production of powerful oxidizing species, mainly hydroxyl radicals ($HO^{\bullet}$), which can attack organic contaminants (Banerjee et al., 2014), such as antibiotics (Mirzaei et al., 2016), until their final mineralization into CO_2 and inorganic ions. Among various photocatalysts, ZnO has received considerable attention owing to its unique characteristics. ZnO is a semiconductor with a large exciton binding energy of 60 meV and a wide band gap of 3.2 eV at room temperature (Lee et al., 2016). It has the ability to absorb over a larger fraction of the solar spectrum compared to other semiconducting metal oxides, plus it is a biocompatible, non-toxic and low-cost material (Zacharakis et al., 2013; Koutantou et al., 2013; Lee et al., 2016). A way to enhance the photocatalytic activity of a catalyst is by controlling its morphological and structural properties (i.e. surface area, pore size distribution, lattice defects, as well as the predominant crystal facets of the nanostructures). In this study, a low-cost, versatile hydrothermal-assisted technique, applicable at industrial scale, was used to develop ZnO materials with augmented photocatalytic activity.

The degradation of SMX by means of photocatalytic oxidation has been widely studied Abellán et al., 2007; Xekoukoulotakis et al., 2011; Lu et al., 2017; Tomara et al., 2019), however ZnO-mediated photocatalysis has been merely investigated and this only under UVC irradiation. In

88 detail, Pourmoslemi et al. (2016) examined the photocatalytic degradation of SMX over ZnO
89 nanoparticles synthesized by a microwave-assisted gel combustion method. Results showed
90 complete removal of SMX using ZnO nanoparticles/UVC irradiation after 6 hours of treatment.
91 Mirzaei et al. (2018a) achieved 90.4% removal of SMX after 60 min of treatment over a
92 synthesized hierarchical magnetic zinc oxide based composite ZnO@g – C_3N_4 (FZG) when
93 irradiated by UVC light. The same group also studied SMX degradation in the presence of
94 fluorinated ZnO nanoparticles (F-ZnO) and under UVC irradiation obtaining 97% SMX removal
95 after 30 min of treatment (Mirzaei et al., 2018b). Previous studies have demonstrated the
96 efficiency of several ZnO/UVC systems in removing SMX from water, however a study
97 investigating the photocatalytic degradation of SMX by a ZnO/UVA system is still missing from
98 literature. UVA lamps constitute a safer and less energy intensive option than UVC light sources,
99 decreasing the environmental impact of photocatalytic treatment. Furthermore, the wide bandgap
100 of ZnO catalysts is one of their key advantages; ZnO has shown augmented absorbance in the
101 UVA region when compared with the benchmark catalyst P25 TiO_2.
102 To this end, the aim of this work was to investigate the fabrication of ZnO nanostructures and
103 test their photocatalytic activity under UVA irradiation for eliminating SMX antibiotic in water.
104 Parameters affecting the synthesis of ZnO catalysts, such as the heating time and pH of the
105 synthesis reaction, were examined. Key operating factors, including catalyst and SMX initial
106 concentration, as well as the type of the water matrix, were studied in order to assess the
107 efficiency of the process.
108

2. Experimental

2.1. Materials

Sulfamethoxazole (SMX; ≥ 99% purity, CAS No. 723-46-6) was purchased from Sigma-Aldrich. Leonardite humic acid (HA) IHSS standard was used. HA stock solution was prepared by dissolving a prescribed amount of HA in 0.1 M NaOH and further diluting it in ultra-pure water (UPW; 18.2 MΩ.cm at 25 °C, ELGA LabWater). Surface water (SW) was collected from Blackford Pond (Edinburgh, UK) (TOC = 13.9 mg/L; pH = 6.8 – 7; conductivity = 0.42 mS/cm) and used without pre-treatment. Tert-butyl alcohol and methanol were obtained from Panreac and Sigma-Aldrich, respectively. Commercial ZnO powder Honeywell Fluka was supplied from Fisher Scientific. All reagents used for the synthesis of ZnO catalysts were of analytical grade that were purchased from Sigma-Aldrich and used as received.

2.2. ZnO synthesis

ZnO nanostructures were prepared using the facile hydrothermal-assisted process described below. Prior to synthesis, 0.2 M $Zn(NO_3)_2.6H_2O$ was added in 125 mL deionised water and allowed to stir for 2 h at room temperature. While the solution was stirred, approx. 1 M NaOH was added drop-wise to adjust the pH to 7.5, 10.5 or 12.5. After 2 h of stirring, 125 mL of the solution was transferred to an autoclave reactor vessel (stainless steel, volume 200 mL Anton Paar) and synthesized in an oven at 200 °C for specific time intervals ranging from 8 to 48 h. White solid precipitates were attained that were collected by consecutive rinse/centrifugation cycles using deionized water. The final ZnO product was dried at 90 °C for 12 h in air.

2.3. Catalyst characterization techniques

The structural features of ZnO were analysed using X-ray powder diffraction (XRD, PANalytical X' pert Pro PW 3040/60, Netherlands) fitted with a Cu radiation (λ = 0.15418 nm) source. XRD analyses were carried out at 45.0 kV and 40.0 mA, from 2θ = 20 to 90° at room temperature. The surface morphology was probed using a field emission scanning electron microscope (SEM, Zeiss-Auriga) at an accelerating voltage of 3 keV. The Brunauer, Emmett and Teller (BET) surface area and N_2 adsorption-desorption isotherms were determined with the use of Micromeritics TRISTAR 3000 (USA). Prior to measurements, ZnO materials were thoroughly degassed at 110 °C for 2 h under continuous N_2 gas flow to remove adsorbed contaminants. The optical properties were probed using a photoluminescence spectrometer (Jobin-Yvon Nanolog) at an excitation wavelength of 330 nm using a xenon lamp (see the electronic supplementary information, ESI).

2.4. Photocatalytic tests

Experiments were conducted in an immersion well, batch-operated, slurry photoreactor, purchased from Ace Glass (Vineland, NJ, USA). UVA irradiation was provided by an 11 W low-pressure blacklight fluorescent lamp (PLS G23, Casell Lighting), emitting predominantly at λ = 365 nm. Potassium ferrioxalate actinometry was applied for the estimation of the incident photon flux received by the reactant solution, which was found to be $4.98 \cdot 10^{-6}$ Einstein/s. In a typical photocatalytic run, 500 mL of SMX solution were introduced in the photoreactor and the appropriate amount of catalyst was added. The obtained slurry solution was continuously stirred magnetically to ensure uniform dispersion of catalyst powder and dissolved oxygen. At the beginning of each experiment, the solution was stirred in the dark for 30 min considering that a

well-adsorbed substrate is more likely to be oxidized by the short-life photogenerated holes on catalyst surface. After that time, the UVA lamp was switched on and samples were withdrawn at regular time intervals, filtered through 0.45 μm polyvinylidene fluoride (PVDF) syringe filters (CM Scientific Ltd) and further analyzed in terms of SMX concentration. All experiments were conducted at room temperature and at the inherent pH of SMX solutions, which remained constant during photocatalytic treatment.

2.5. Analytical techniques

SMX concentration in filtrate samples was measured by means of a high performance liquid chromatography (HPLC) system (S200 Pump, S225 Autosampler, Perkin Elmer) coupled with a diode array detector (S200 EP, Perkin Elmer). Separation was performed on a reverse phase C18 analytical column (Luna Phenomenex, 5μm, 250 × 4.6 mm) in isocratic elution mode. The HPLC method for SMX measurement was obtained from Özkal et al. (2017). The mobile phase was a mixture of acidified water (pH ~ 3) and acetonitrile (60/40, v/v), eluted at a flow rate of 1 mL/min. The detection wavelength was set to 270 nm and the injection volume to 40 μL. The retention time of the detected SMX was 6.27 min. Since humic acid (HA) solution with a UV absorbance around 254 nm (Rodríguez et al., 2016) is used in this work as a water matrix, it is important to note that the presence of HA could not interfere with the HPLC method used in this study for SMX detection, and that it had a negligible impact on the separation of SMX.

3. Results and Discussion

3.1. Catalyst characterization

Figure 1 displays the XRD patterns of ZnO nanostructures synthesized at different pH at 200 °C for 8 h. All the diffraction peaks can be indexed to the standard wurtzite ZnO form (JCPDS No. 36-1451). The absence of additional peaks indicates the lack of impurities, thus validating the quality of the as-prepared ZnO nanostructures. Furthermore, a size–dependent spreading of the curve is observed with the increase of the synthesis pH; a clear peak shift to higher angles takes place, when pH increases from 7.5 to 12.5 (Figure 1b). The average crystallite sizes, estimated by the Scherer formula (Mhlongo et al., 2015), are 39.31 and 33.68 nm for pH 7.5 and 12.5, respectively.

Figure 1

The N_2 adsorption/desorption isotherms of ZnO catalysts, shown in Figure 2, reveal a type IV behaviour with pore diameter in the range of 4 – 100 nm. Both S_{BET} and pore diameter depend on the pH of the synthesis reaction; S_{BET} increases from 4.852 ± 0.101 m^2/g at pH 7.5 to 7.547 ± 0.113 m^2/g at pH 12.5 for the same synthesis reaction time of 8 h. This is also confirmed by SEM and XRD analyses (Figures 1 and 3), which reveal reduction of crystallite size and further morphological and textural transformations of ZnO structures at higher reaction pH values.

Figure 2

The SEM micrographs of ZnO catalysts are presented in Figure 3. As can be seen in the low resolution of Figure 3a, synthesis of ZnO at pH 7.5, leads to the growth of nanorods on its surface, which are nearly all aligned towards the same direction. The higher resolution inset graph of Figure 3a further reveals the hexagonal nature of these nanorods. The average diameter and length of the nanorods are roughly 50 nm and 1 μm, respectively. ZnO synthesis at higher pH (i.e. 12.5) results in the formation of nanoplatelets with average diameter approx. 75 nm (Figure 3b).

Figure 3

3.2. Effect of ZnO synthesis route on SMX degradation

One way to enhance the photocatalytic activity of materials is via morphological and structural modification, which can be achieved by altering synthesis parameters. This study investigates the effect of two key parameters, the pH of the synthesis reaction and the heating time, on the photocatalytic activity of ZnO. Figure 4 shows the degradation of SMX in the presence of ZnO catalysts synthesized at different pH (i.e. 7.5, 10.5 and 12.5) and heated for 24 h at 200 ^{o}C during synthesis. As can be seen, the photocatalytic degradation of SMX decreases gradually with the increase of synthesis reaction pH. In detail, SMX removal percentages in the presence of ZnO catalysts synthesized at pH 7.5, 10.5 and 12.5 are 58, 55 and 44%, respectively. The photocatalytic degradation of SMX was found to fit very well with the pseudo-first-order kinetics with the coefficient of linear regression of data fitting, R^2, being > 0.99.The pseudo-first-

order kinetic constants, k_{app} were calculated at 0.015, 0.013 and 0.009 min^{-1} for SMX degradation over ZnO synthesized at 7.5, 10.5 and 12.5, respectively. It becomes clear that the use of ZnO nanostructures synthesized at acidic conditions enhances photocatalytic performance. This can be explained by the higher relative concentration of lattice defects that is observed at lower pH values and leads to improved charge transportation and thus higher process efficiency (Nkosi et al., 2014). Based on the photoluminescence study that was carried out for the ZnO under study (Figure S1), it is evident that the relative concentration of oxygen vacancies (V_O) [estimated from the relative intensity of visible emission and ultraviolet (Vis(V_O)/UV)] decreases from 6.85 to 4.09 and further to 0.99 as synthesis reaction pH increases from 7.5 to 10.5 and further to 12.5, respectively.

V_O leads to the creation of unpaired electrons acting as donors and it alters the adsorption behavior of O_2 and H_2O on ZnO surface. The generated pairs of electron holes can directly react with organic substances, (Eq. (5), or indirectly by producing free radicals, Eqs. (2)–(4) (Mirzaei et al., 2016) .

$$ZnO + hv \rightarrow ZnO\ (h_{VB}^{+} + e_{CB}^{-}) \quad (1)$$

$$e_{CB}^{-} + O_{2(ads)} \rightarrow O_2^{\bullet -} \quad (2)$$

$$h_{VB}^{+} + H_2O_{(ads)} \rightarrow H^{+} + OH^{\bullet} \quad (3)$$

$$h_{VB}^{+} + HO^{-}(ads) \rightarrow OH^{\bullet} \quad (4)$$

$$h_{VB}^{+} + organic\ substance\ (OS) \rightarrow OS^{\bullet +} \rightarrow Oxidized\ products \quad (5)$$

Figure 4

The effect of heating time during ZnO synthesis on its photocatalytic activity was then assessed. For this purpose, ZnO catalysts were prepared applying different heating times (i.e. 8, 12, 24, and 48 h) at 200 ^{o}C and reaction pH 7.5. As can be seen in Figure 5, the heating time has a negative effect on the ZnO photocatalytic performance. For example, SMX removal in the presence of 8 h-heated ZnO is 84%, after 60 min of treatment, while decreases to 56% when ZnO heated for 48 h is used. Considering that not any structural change occurs during the increase of the synthesis reaction time, this behavior can be attributed to the decrease of the active surface area from 4.852 ±0.101 m²/g (at 8 h) to 0.790 ±0.104 m²/g (at 48 h) that is observed as the crystallite sizes increase with heating time. As a result, SMX removal decreases, since there is less surface area to facilitate photocatalytic reactions (Wang et al., 2012). This trend can be also justified by the reduction of lattice defects, such as V_O, because the crystal quality of the material improves with reaction time.

The photocatalytic degradation of SMX was further evaluated in the presence of ZnO (Fluka), at the same operational conditions, to establish a comparison against a commercially available photocatalyst. In this case, 99.9% of SMX was removed within 40 min of treatment. The observed difference in photocatalytic activity can be attributed to the higher adsorption capacity of ZnO (Fluka) compared to the synthesized ZnO materials; after 30 min in the dark, 13.1% of SMX has been adsorbed on ZnO (Fluka), whereas the respective percentages for the novel catalysts are in the range of 1.6 – 7.2%, Adsorption capacity increases with surface area, for that reason ZnO-8h@7.5pH and ZnO-8h@12.5pH, the two catalysts with the highest S_{BET} (Figure 2), are tested in the following experiments to optimize the process and explore their capacity in different water matrices.

262 Figure 5

263

264 **3.3. Effect of initial concentration of SMX**

265 To evaluate the effect of the initial SMX concentration on photocatalytic performance, 5, 10, and
266 20 mg/L of SMX were applied in the presence of 200 mg/L ZnO heated for 8 h at pH 7.5 (noted
267 as ZnO-8h@7.5pH). As can be seen in Figure 6a, when the initial concentration of SMX
268 increases from 5 to 20 mg/Lremoval efficiency decreases from 90% (k_{app} = 0.039 min^{-1}) to
269 62.6% (k_{app} = 0.016 min^{-1}). At a fixed catalyst loading, efficiency is dictated by catalyst's active
270 sites to organic molecules ratio. At relatively low solute concentration, the active sites provided
271 by the semiconductor are in excess and can uptake most of the organic molecules, resulting at
272 higher removal rates. Increase of the initial SMX concentration leads to an excessive coverage of
273 the photocatalyst surface by SMX molecules and reaction by-products, which compete for the
274 active sites of the catalyst, as well as, for the photogenerated hydroxyl radicals, affecting the
275 degradation rates and thus explaining the above findings. SEM graphs of the catalyst after 60
276 min of photocatalytic treatment confirm the extent of surface coverage and further reveal the
277 transformation of surface morphology after contact with organic molecules (in this case SMX)
278 from nanorods (Figure 3a) to nanoparticles (Figure 6b, 6c, 6d). As shown in Figure 6b, after
279 treatment of the solution containing 5 mg/L SMX there are still some nanorods on catalyst
280 surface not yet occupied by SMX molecules However, when the initial concentration of SMX
281 increases to 10 or 20 mg/L, the surface morphology is completely dominated by nanoparticles
282 (Figure 6c and 6d) indicating the complete coverage of catalyst surface by SMX molecules and
283 reaction by-products.

284

285 Figure 6

286

287 **3.4. Effect of catalyst concentration**

288 To investigate the effect of catalyst loading on process efficiency, different concentration of
289 ZnO-8h@7.5pH catalyst (i.e. 100, 150 and 200 mg/L) were used for the degradation of 10 mg/L
290 SMX. SMX removal was found to be 72% (k_{app} = 0.021 min^{-1}), 73% (k_{app} = 0.022 min^{-1}) and
291 83% (k_{app} = 0.03 min^{-1}) in the presence of 100, 150 and 200 mg/L ZnO, respectively after 60 min
292 of treatment (data not shown). At higher amounts of catalyst, the increased number of available
293 active sites results in higher generation of radicals, which are responsible for the photocatalytic
294 oxidation, thus explaining the obtained results (Patil et al., 2010).

295

296 **3.5. Effect of water matrix**

297 Photocatalytic efficiency in environmentally relevant samples, such as surface or waste water,
298 typically varies from that in ultrapure water (UPW) due to the presence of several inorganic and
299 organic constituents that alter degradation kinetics. Humic acid (HA) represents a large fraction
300 of natural organic matter (NOM) in surface waters with concentrations ranging from 2 to 10
301 mg/L (Alrousan et al., 2009). Taking this into account, experiments were carried out in UPW
302 spiked with 2 mg/L HA and in surface water (SW) to assess the effect of water matrix on the
303 photocatalytic removal of SMX. As can be seen in Figure 7, the degradation yield in SW is
304 considerably lower than in UPW; after 60 min of photocatalytic treatment, 47.4% of SMX is
305 degraded in UPW, whereas removal efficiency decreases by almost four times (12.5%) in SW.
306 NOM, HCO_3^-, Cl^-, SO_4^{2-}, PO_4^{3-}, etc., present in SW, may suppress reaction kinetics via

competition with SMX for the reactive oxygen species, conversion of hydroxyl radicals into species of lower oxidation potential, and/or adsorption on catalyst surface, thus explaining the obtained results (Rincón and Pulgarin, 2004; Antonopoulou et al., 2015). On the other hand, SMX removal is greatly enhanced in the presence of HA; 10 mg/L of SMX are completely removed within 60 min in HA matrix, which is almost the double yield of that in UPW. Interestingly, the ability of HA to sensitize colloidal ZnO has been previously demonstrated (Selli et al., 1996; Delgado-Balderas et al., 2012). Selli et al. (1996) have shown that HA adsorbed onto the ZnO surface sensitize Cr(VI) photoreduction to Cr(III), as well as, the competitive photoreduction of molecular oxygen leading to hydrogen peroxide, therefore enhancing photocatalytic efficiency. HAs are electron-rich compounds that can easily scavenge the holes produced on semiconductor's valence band, thus reducing the recombination rate of the photogenerated electron-hole pairs. Moreover, electron transfer to the conduction band of the semiconductor may also occur due to the excitation of HAs adsorbed onto catalyst surface upon UV and visible irradiation, accelerating redox reactions and leading to higher reaction rates (Selli et al. 1996). Therefore, the increased SMX degradation rate in the presence of HA might be attributed to the photosensitizing effect of adsorbed HA onto the surface of ZnO nanoparticles. Based on the results shown in Figure 7 (i.e. the huge difference in SMX removal in HA and SW matrices), concerns can arise on whether HA solutions, which are commonly used at lab-scale to simulate natural water matrices (e.g. surface waters), are representative of real environmental conditions. Besides, the long-term exposure to high concentrations (i.e. >50 mg/L) of HA in water has been found to be toxic to endothelial cells and to cause adverse effects on public health (Kihara et al., 2014).

330 Figure 7

331

332 To assess the effect of water matrix (i.e. UPW, HA, SW) on catalyst surface, SEM analyses were
333 carried out on the used ZnO materials (Figure 8). It can be observed that after 60 min of
334 photocatalytic treatment in the presence of several organic substances (i.e. SMX, HA or NOM),
335 all nanoplatelets of the pristine ZnO materials (Figure 3b) have transformed into nanoparticles.
336 Nevertheless, differences are observed in the size and the texture of the nanoparticles. For
337 example, when 10 mg/L SMX is treated in HA matrix (Figure 8c) the size of the nanoparticles is
338 bigger than in the case of SMX treatment in UPW (Figure 8a), and this is also confirmed by the
339 evolution of crystallite size after photocatalysis, as shown in Figure 9. Moreover, when SMX is
340 treated in SW matrix (Figure 8e), nanoplatelets are altered to fluffy nanoparticles showing some
341 porous behaviour. Also, while the morphology of ZnO in Figure 8e has changed to nanoparticles,
342 its texture is different than that of SW alone (Figure 8d), since nanoparticles form an island on
343 catalyst surface.

344

345 Figure 8

346

347 Figure 9

348

349 **3.6. Oxidation mechanism**

Additional experiments were carried out in the presence of $HO^{\bullet}$ quenchers to evaluate the contribution of $HO^{\bullet}$ on the photocatalytic degradation of SMX. For this purpose, solution of 1 M *tert*-butyl alcohol or methanol was used. $HO^{\bullet}$ react with *tert*-butyl alcohol and methanol according to Eqs. (6) and (7), respectively. SMX degradation was found to be negligible in the presence of *tert*-butyl alcohol or methanol (data not shown) suggesting that $HO^{\bullet}$ are the major oxidizing species. Furthermore, it was observed that SMX removal, after 60 min of treatment, was slightly higher in the presence of *tert*-butyl alcohol (i.e. 20%) than methanol (i.e. 7%). This is probably due to the fact that methanol reacts at a higher rate with $HO^{\bullet}$ ($k' = 9.7 \cdot 10^8$ M^{-1} s^{-1}, Eq. (7)) than *tert*-butyl alcohol ($k' = (3.8\text{-}7.6) \cdot 10^8$ M^{-1} s^{-1}, Eq. (6)) (Matta et al., 2011), quenching $HO^{\bullet}$ faster and thus leaving very few available to react with other organics (i.e. SMX) even from the beginning of treatment.

$$HO^{\bullet} + (CH_3)_3COH \rightarrow \cdot CH_2(CH_3)_2COH + H_2O \quad (1)$$

$$HO^{\bullet} + CH_3OH \rightarrow H_2O + \cdot CH_2OH \quad (2)$$

4. Conclusions

This work reports for first time the degradation of sulfamethoxazole (SMX) under UVA irradiation and over novel ZnO nanomaterials. It was found that the pH of the ZnO synthesis solution significantly affects the morphology of the prepared catalysts and consequently their photocatalytic activity. SMX photo-degradation fits well with pseudo-first-order reaction kinetics, while photocatalytic efficiency increases when the initial SMX concentration is decreased. In all cases, it was observed that after photocatalytic treatment of organic molecules (i.e. SMX, humic acids or natural organic matter), the nanostructure of the catalyst surface was altered from nanorods (or nanoplatelets) to nanoparticles. SMX degradation was assessed in

371 humic acid solution (HA) and surface water (SW) to resemble real environmental conditions. It
372 was found that SMX removal was substantially decreased in SW but greatly enhanced in HA due
373 to the photosensitizing effect of adsorbed HA onto the surface of ZnO nanoparticles, thus raising
374 concerns on whether HA can be widely adopted as a simulant of natural waters (e.g. SW).
375 Considering the encouraging results obtained with the use of the ZnO materials under study,
376 future work should consider the identification of the reaction by-products formed during the
377 photocatalytic degradation of SMX under UVA irradiation and the corresponding toxicity
378 evolution.

379

380

381 **References**

382 Abellán M.N., Bayarri B., Giménez J., Costa J., Photocatalytic degradation of sulfamethoxazole
383 in aqueous suspension of TiO2, Appl. Catal. B Environ. 74 (2007) 233–241.

384 Alrousan D., Dunlop P.S.M., McMurray T.A., Byrne J.A., Photocatalytic inactivation of E. coli
385 in surface water using immobilised nanoparticle TiO2 films, Water Res. 43 (2009) 47–54.

386 Antonopoulou M., Skoutelis C.G., Daikopoulos C., Deligiannakis Y., Konstantinou I.K., Probing
387 the photolytic-photocatalytic degradation mechanism of DEET in the presence of natural
388 or synthetic humic macromolecules using molecular-scavenging techniques and EPR
389 spectroscopy, J. Environ. Chem. Eng. 3 (2015) 3005–3014.

390 Banerjee S., Pillai S.C., Falaras P., O'shea K.E., Byrne J.A., Dionysiou D.D., New insights into
391 the mechanism of visible light photocatalysis, J. Phys. Chem. Lett. 5 (2014)

392 Barbosa M.O., Moreira N.F.F., Ribeiro A.R., Pereira M.F.R., Silva A.M.T., Occurrence and
393 removal of organic micropollutants: An overview of the watch list of EU Decision
394 2015/495, Water Res. 94 (2016) 257–279.

395 Byrne C., Subramanian G., Pillai S.C., Recent advances in photocatalysis for environmental
396 applications, J. Environ. Chem. Eng. 6 (2018) 3531–3555.

397 Delgado-Balderas R., Hinojosa-Reyes L., Guzmán-Mar J.L., Garza-González M.T., López-
398 Chuken U.J., Hernández-Ramírez A., Photocatalytic reduction of Cr(VI) from agricultural
399 soil column leachates using zinc oxide under UV light irradiation, Environ. Technol. 33
400 (2012) 2673–2680.

401 Fatta-Kassinos D., Meric S., Nikolaou A., Pharmaceutical residues in environmental waters and
402 wastewater: Current state of knowledge and future research, Anal. Bioanal. Chem. 399
403 (2011) 251–275.

404 Giannakis S., Le T.T.M., Entenza J.M., Pulgarin C., Solar photo-Fenton disinfection of 11
405 antibiotic-resistant bacteria (ARB) and elimination of representative AR genes. Evidence
406 that antibiotic resistance does not imply resistance to oxidative treatment, Water Res. 143
407 (2018) 334–345.

408 Jiang H., Zhang D., Xiao S., Geng C., Zhang X., Occurrence and sources of antibiotics and their
409 metabolites in river water, WWTPs, and swine wastewater in Jiulongjiang River basin,
410 south China, Environ Sci Pollut Res 20 (2013) 9075–9083.

411 Karaolia P., Michael-Kordatou I., Hapeshi E., Drosou C., Bertakis Y., Christofilos D., Armatas
412 G.S., Sygellou L., Schwartz T., Xekoukoulotakis N.P., Fatta-Kassinos D., Removal of
413 antibiotics, antibiotic-resistant bacteria and their associated genes by graphene-based

TiO2composite photocatalysts under solar radiation in urban wastewaters, Appl. Catal. B Environ. 224 (2018) 810–824. doi:10.1016/j.apcatb.2017.11.020.

Kihara Y, Yustiawati, Tanaka M, Gumiri S, Ardianor, Hosokawa T, Tanaka S, Saito T, Kurasaki M, Mechanism of the Toxicity Induced by Natural Humic Acid on Human Vascular Endothelial Cells, Environ Toxicol 29(8) (2014) 916 – 925.

Koutantou V., Kostadima M., Chatzisymeon E., Frontistis Z., Binas V., Venieri D., Mantzavinos D., Solar photocatalytic decomposition of estrogens over immobilized zinc oxide, Catal. Today. 209 (2013) 66–73.

Lee K.M., Lai C.W., Ngai K.S., Juan J.C., Recent developments of zinc oxide based photocatalyst in water treatment technology: A review, Water Res. 88 (2016) 428–448.

Lee S.-H., Kim K.-H., Lee M., Lee B.-D., Detection status and removal characteristics of pharmaceuticals in wastewater treatment effluent, J Water Process Eng. 31 (2019).

Lin C.-C., Wu M.-S., Performance of a large reactor in degrading sulfamethazine in water using UV and persulfate, J Water Process Eng. 31 (2019).

Lu N., Yeh Y.-P., Wang G.-B., Feng T.-Y., Shih Y., Chen D., Dye-sensitized TiO2-catalyzed photodegradation of sulfamethoxazole under blue or yellow light, Environ Sci Pollut Res 24 (2017) 489–499.

Lupo A., Coyne S., Berendonk T.U., Origin and evolution of antibiotic resistance: the common mechanisms of emergence and spread in water bodies, Front. Microbiol. 3 (2012) 18.

Martin-Laurent F., Topp E., Billet L., Batisson I., Malandain C., Besse-Hoggan P., Morin S., Artigas J., Bonnineau C., Kergoat L., Devers-Lamrani M., Pesce S., Environmental risk

435 assessment of antibiotics in agroecosystems: ecotoxicological effects on aquatic microbial
436 communities and dissemination of antimicrobial resistances and antibiotic biodegradation
437 potential along the soil-water continuum, Environ. Sci. Pollut. Res. 26 (2019) 18930–
438 18937.

439 Matta R., Tlili S., Chiron S., Barbati S., Removal of carbamazepine from urban wastewater by
440 sulfate radical oxidation, Environ. Chem. Lett. 9 (2011) 347–353.

441 Mhlongo G.H., Motaung D.E., Kortidis I., Mathe N.R., Ntwaeaborwa O.M., Swart H.C.,
442 Mwakikunga B.W., Ray S.S., Kiriakidis G., A study on the sensing of NO2 and O2
443 utilizing ZnO films grown by aerosol spray pyrolysis, Mater. Chem. Phys. 162 (2015)
444 628–639.

445 Michael I., Rizzo L., McArdell CS., Manaia CM., Merlin C., Schwartz T., Dagot C., Fatta-
446 Kassinos D., Urban wastewater treatment plants as hotspots for the release of antibiotics
447 in the environment: a review, Water Res. 47 (2013) 957–995.

448 Mirzaei A., Chen Z., Haghighat F., Yerushalmi L., Removal of pharmaceuticals and endocrine
449 disrupting compounds from water by zinc oxide-based photocatalytic degradation: A
450 review, Sustain. Cities Soc. 27 (2016) 407–418.

451 Mirzaei A., Yerushalmi L., Chen Z., Haghighat F., Photocatalytic degradation of
452 sulfamethoxazole by hierarchical magnetic ZnO@g-C3N4: RSM optimization, kinetic
453 study, reaction pathway and toxicity evaluation, J. Hazard. Mater. 359 (2018a) 516–526.

454 Mirzaei A., Yerushalmi L., Chen Z., Haghighat F., Guo J., Enhanced photocatalytic degradation
455 of sulfamethoxazole by zinc oxide photocatalyst in the presence of fluoride ions:
456 Optimization of parameters and toxicological evaluation, Water Res. 132 (2018b) 241–

251.

Nkosi SS., Kortidis I., Motaung DE., Makgwane PR., Ndwandwe OM., Ray SS., Kiriakidis G., An instant photo-excited electrons relaxation on the photo-degradation properties of TiO2− x films., J. Photochem. Photobiol. A Chem. 293 (2014) 72–80.

OECD, Antimicrobial Resistance: Policy Insights, OECD. (2016).

Özkal C.B., Frontistis Z., Antonopoulou M., Konstantinou I., Mantzavinos D., Meriç S., Removal of antibiotics in a parallel-plate thin-film-photocatalytic reactor: Process modeling and evolution of transformation by-products and toxicity, J. Environ. Sci. 60 (2017) 114–122.

Patil A.B., Patil K.R., Pardeshi S.K., Ecofriendly synthesis and solar photocatalytic activity of S-doped ZnO, J. Hazard. Mater. 183 (2010) 315–323.

Pourmoslemi S., Mohammadi A., Kobarfard F., Assi N., Photocatalytic removal of two antibiotic compounds from aqueous solutions using ZnO nanoparticles, Desalin. Water Treat. 57 (2016) 14774–14784.

Ribeiro R.S., Frontistis Z., Mantzavinos D., Venieri D., Antonopoulou M., Konstantinou I., Silva A.M.T., Faria J.L., Gomes H.T., Magnetic carbon xerogels for the catalytic wet peroxide oxidation of sulfamethoxazole in environmentally relevant water matrices, Appl. Catal. B Environ. 199 (2016) 170–186.

Rincón A.G., Pulgarin C., Effect of pH, inorganic ions, organic matter and H2O2 on E. coli K12 photocatalytic inactivation by TiO2: Implications in solar water disinfection, Appl. Catal. B Environ. 51 (2004) 283–302.

478 Rodríguez F.J., Schlenger P., García-Valverde M., Monitoring changes in the structure and
479 properties of humic substances following ozonation using UV-Vis, FTIR and 1H NMR
480 techniques, Science of The Total Environment 541 (2016) 623-637.

481 Selli E., De Giorgi A., Bidoglio G., Humic acid-sensitized photoreduction of Cr(VI) on ZnO
482 particles, Environ. Sci. Technol. 30 (1996) 598–604.

483 Tomara T., Frontistis Z., Petala A., Mantzavinos D., Photocatalytic performance of Ag2O
484 towards sulfamethoxazole degradation in environmental samples, J Environ Chem Engin
485 7 (2019) 103177.

486 Wang Z.X. W., Lu C., Ni Y., Su M., Huang W., Preparation and characterization of visible-light-
487 driven N–F–Ta tri-doped TiO2 photocatalysts., Appl. Surf. Sci. 258 (2012) 8696–8703.

488 Xekoukoulotakis N.P., Drosou C., Brebou C., Chatzisymeon E., Hapeshi E., Fatta-Kassinos D.,
489 Mantzavinos D., Kinetics of UV-A/TiO2 photocatalytic degradation and mineralization of
490 the antibiotic sulfamethoxazole in aqueous matrices, Catal. Today. 161 (2011) 163–168.

491 Zacharakis A., Chatzisymeon E., Binas V., Frontistis Z., Venieri D., Matzavinos D., Solar
492 photocatalytic degradation of bisphenol A on immobilized ZnO or TiO2, Int. J.
493 Photoenergy. (2013).

494

List of Figures

Figure 1. (a) XRD patterns of ZnO nanostructures synthesized at pH 7.5 and 12.5, and (b) high magnification showing a (101) plane with peak shift.

Figure 2. The N_2 adsorption/desorption isotherms of ZnO prepared at pH (a) 7.5 and (b) 12.5.

Figure 3. SEM micrographs of ZnO nanostructures prepared at (a) pH 7.5 and heated for 8 h, and (b) pH 12.5 and heated for 8 h.

Figure 4. Effect of the pH of the ZnO synthesis reaction on the photocatalytic degradation of SMX (C_0 = 10 mg/L, C_{ZnO} = 200 mg/L, ZnO heating time: 24 h).

Figure 5. Effect of catalyst's heating time at 200 ^oC on the photocatalytic degradation of SMX (C_0 = 10 mg/L, C_{ZnO} = 200 mg/L, catalysts' synthesis reaction pH = 7.5).

Figure 6. (a) Effect of initial SMX concentration on its photocatalytic degradation (ZnO-8h@7.5pH, C_{ZnO} = 200 mg/L), (b) SEM micrographs of ZnO-8h@7.5pH after 60 min of treatment at initial SMX concentration of 5 mg/L, (c) 10 mg/L, and (d) 20 mg/L.

Figure 7. Effect of water matrix on the photocatalytic degradation of SMX (C_0 = 10 mg/L, C_{ZnO} = 200 mg/L, catalyst: ZnO-8h@12.5pH).

Figure 8. SEM micrographs of ZnO-8h@12.5pH after 60 min of treatment in the presence of (a) 10 mg/L SMX in UPW, (b) HA matrix, (c) 10 mg/L SMX in HA matrix, (d) SW matrix, and (e) 10 mg/L SMX in SW matrix.

Figure 9. Evolution of the size of crystallite as a function of SMX initial concentrations and the type of the water matrix.

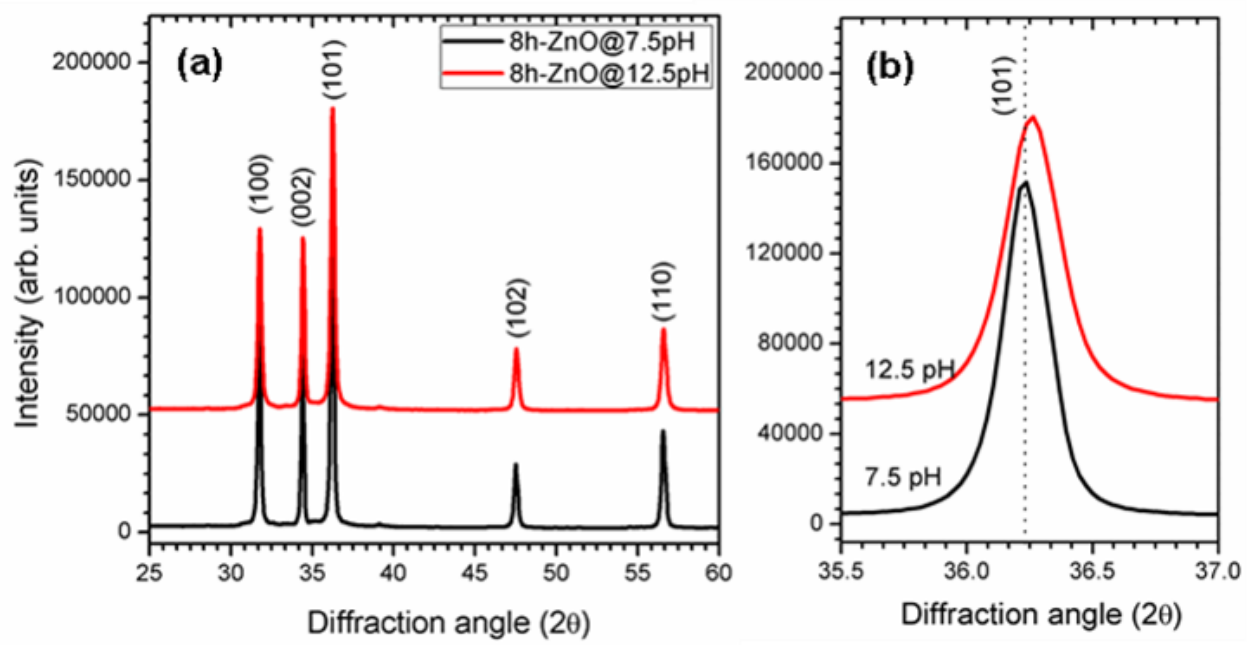

Figure 1. (a) XRD patterns of ZnO nanostructures synthesized at pH 7.5 and 12.5, and (b) high magnification showing a (101) plane with peak shift.

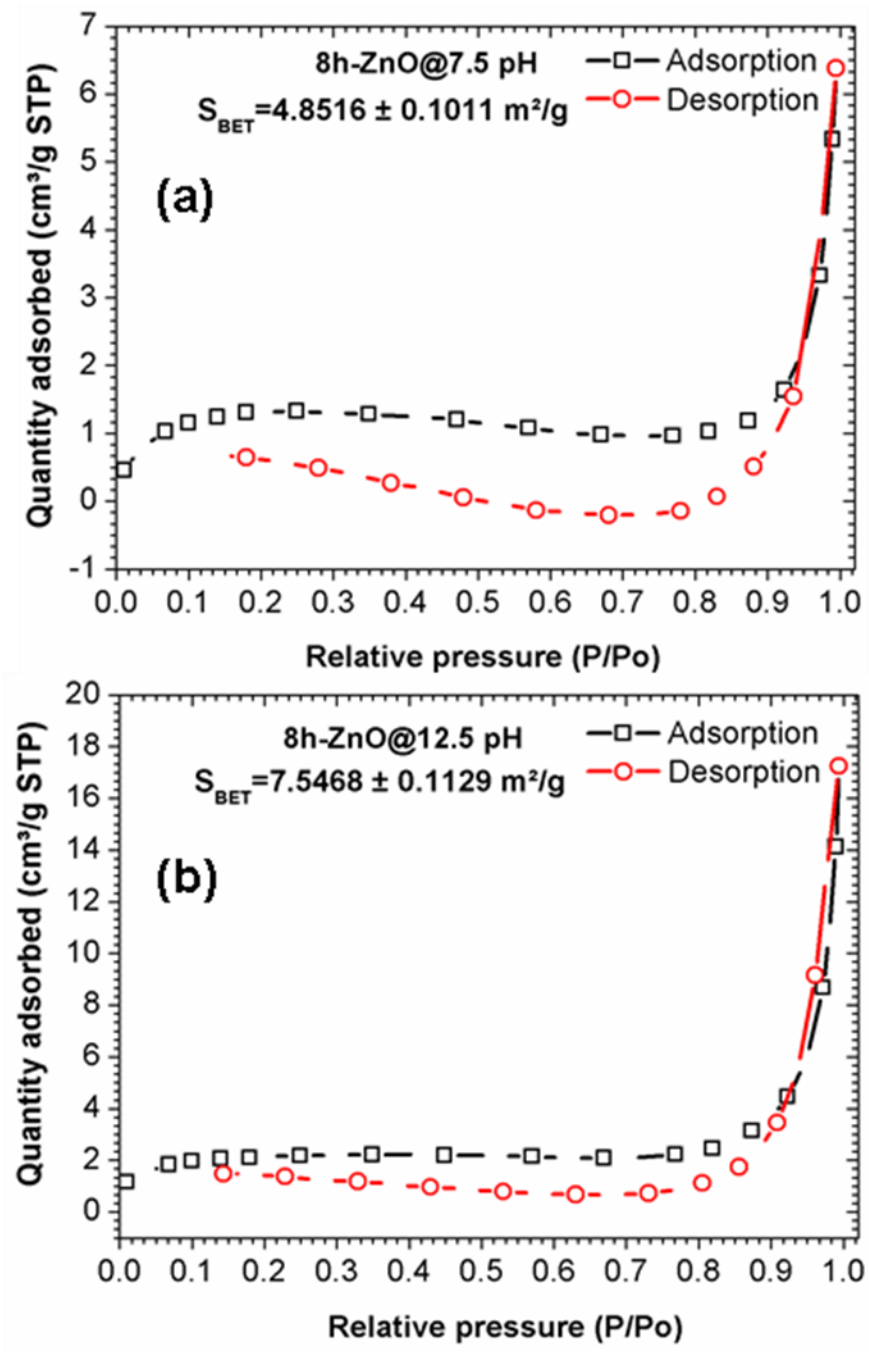

528

529 **Figure 2.** The N_2 adsorption/desorption isotherms of ZnO prepared at pH (a) 7.5 and (b) 12.5.

530

531

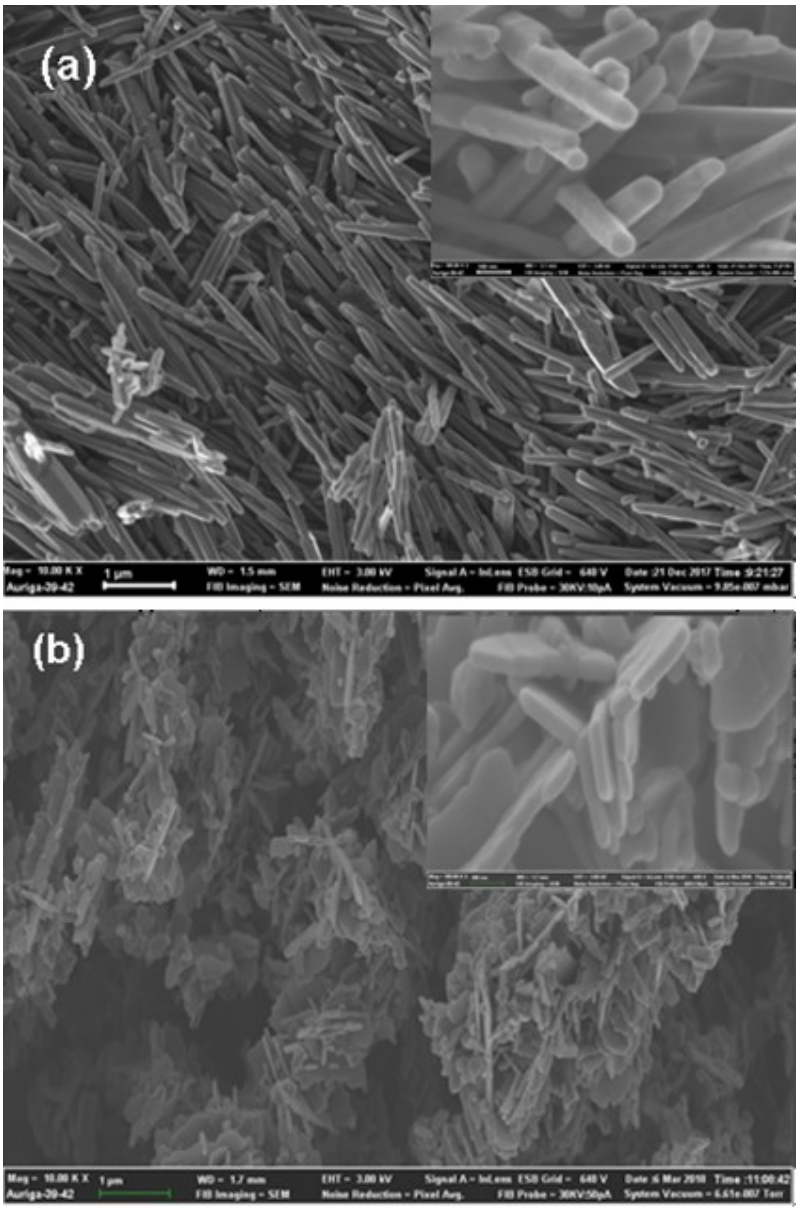

532

533 **Figure 3.** SEM micrographs of ZnO nanostructures prepared at (a) pH 7.5 and heated for 8 h,

534 and (b) pH 12.5 and heated for 8 h.

535

536

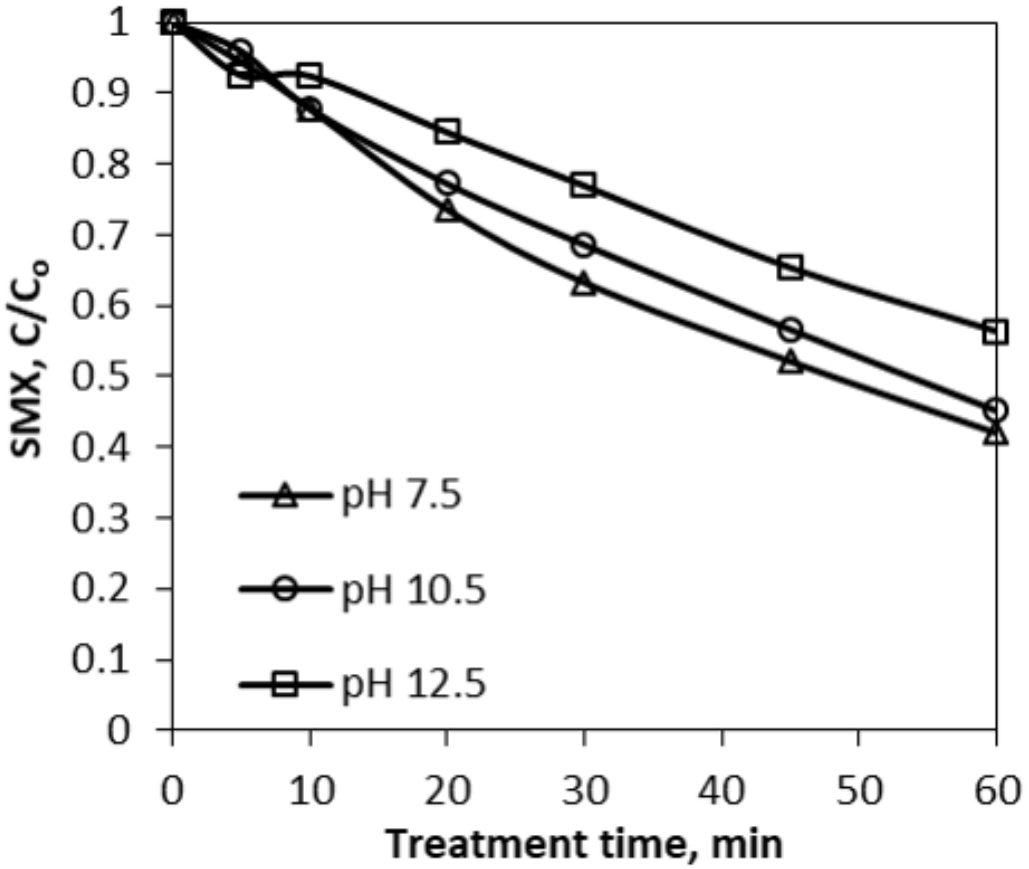

537

538 **Figure 4.** Effect of the pH of the ZnO synthesis reaction on the photocatalytic degradation of

539 SMX (C_0 =10 mg/L, C_{ZnO} = 200 mg/L, ZnO heating time: 24 h).

540

541

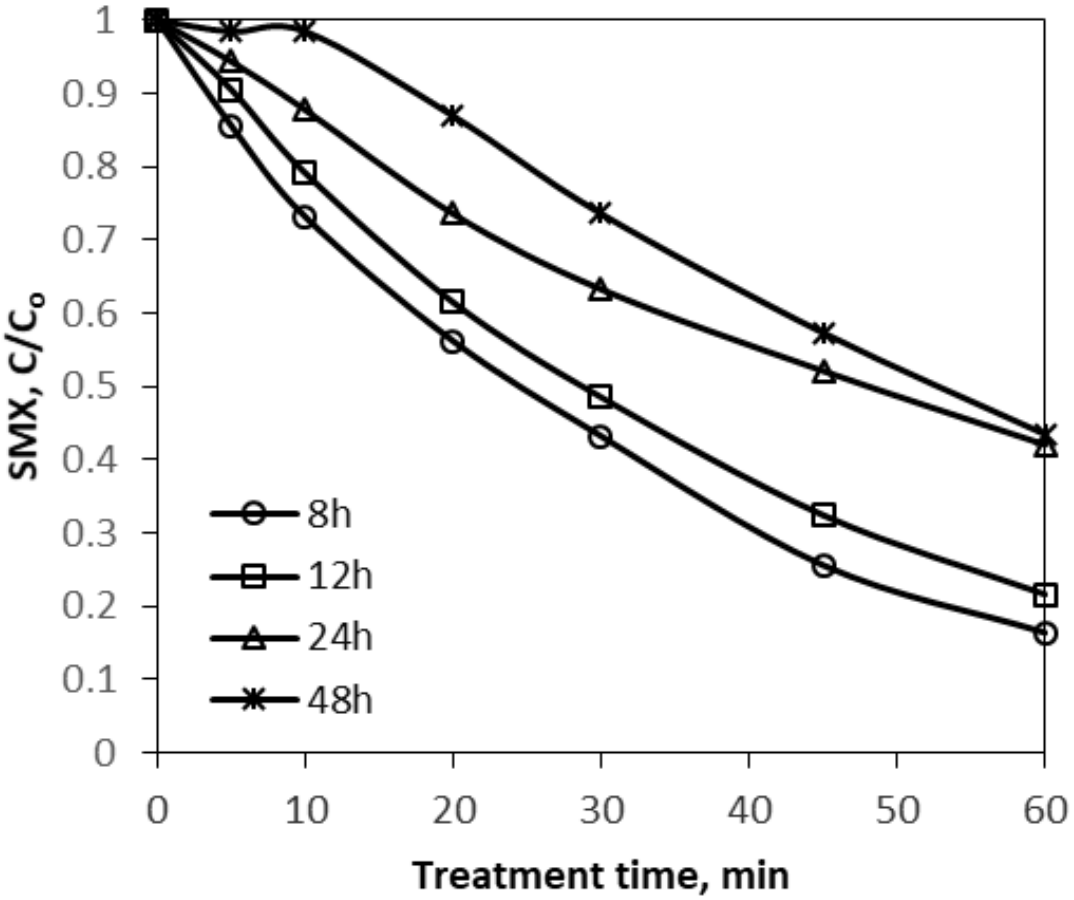

Figure 5. Effect of catalyst's heating time at 200 ^{o}C on the photocatalytic degradation of SMX (C_0 = 10 mg/L, C_{ZnO} = 200 mg/L, catalysts' synthesis reaction pH = 7.5).

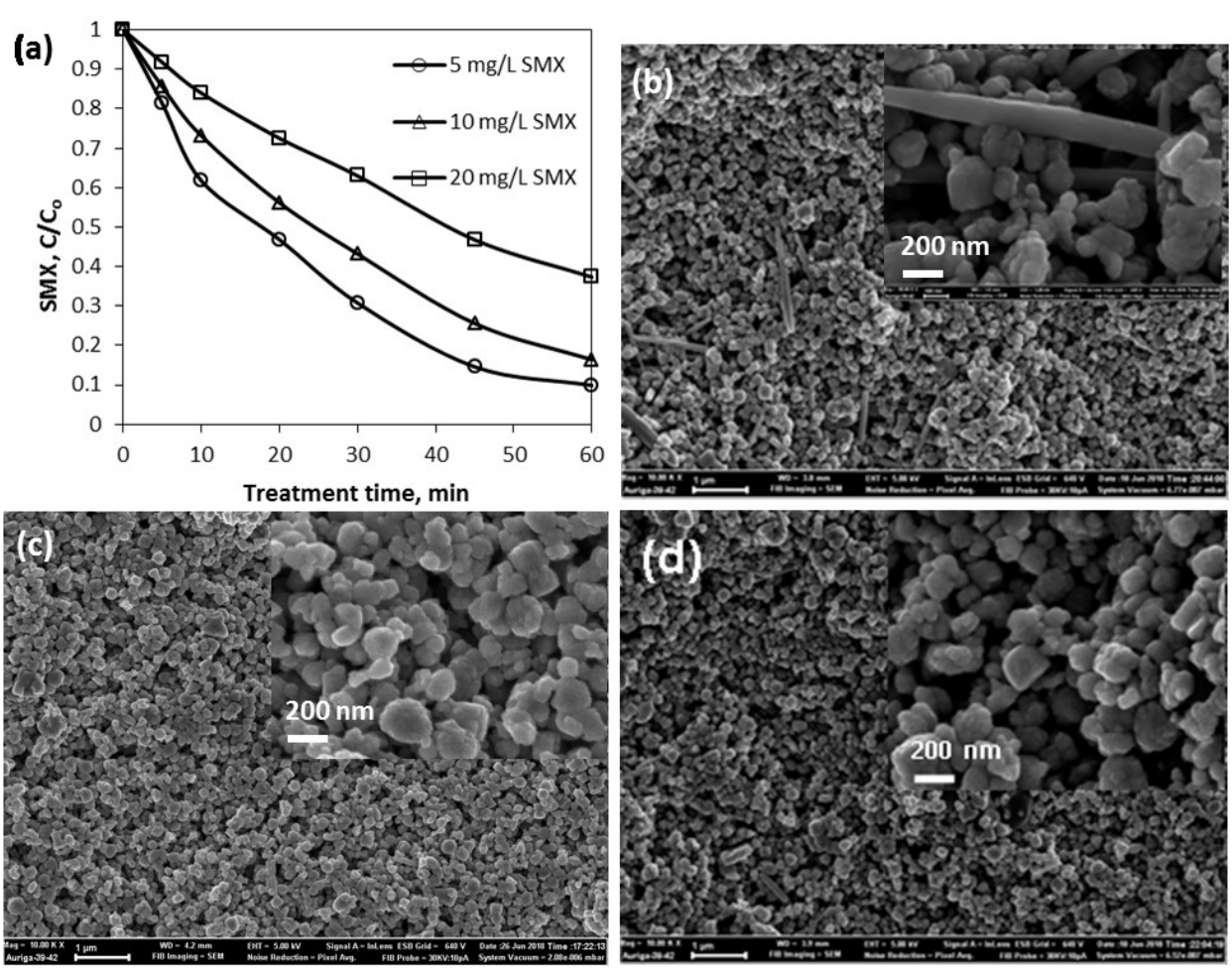

548

549 **Figure 6.** (a) Effect of initial SMX concentration on its photocatalytic degradation (ZnO-
550 8h@7.5pH, C_{ZnO} = 200 mg/L), (b) SEM micrographs of ZnO-8h@7.5pH after 60 min of
551 treatment at initial SMX concentration of 5 mg/L, (c) 10 mg/L, and (d) 20 mg/L.

552

553

554

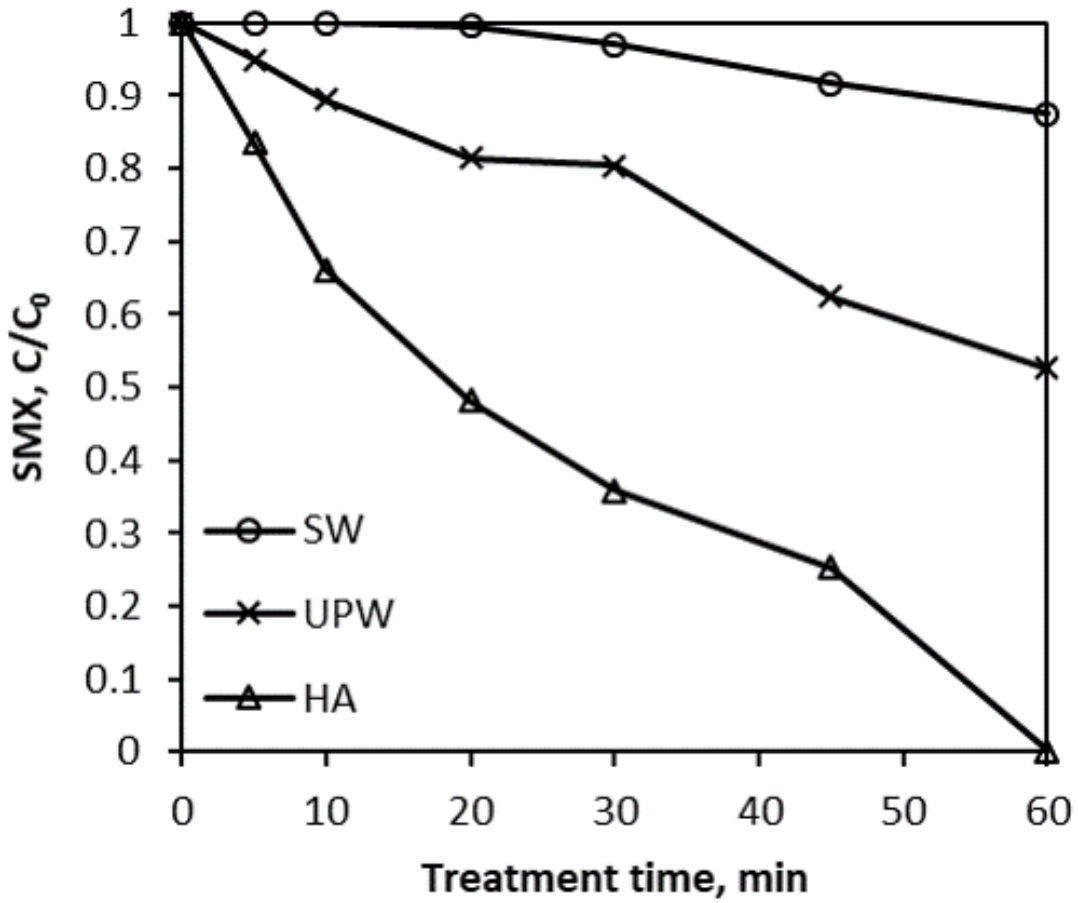

555

556 **Figure 7.** Effect of water matrix on the photocatalytic degradation of SMX (C_0 = 10 mg/L, C_{ZnO}

557 = 200 mg/L, catalyst: ZnO-8h@12.5pH).

558

559

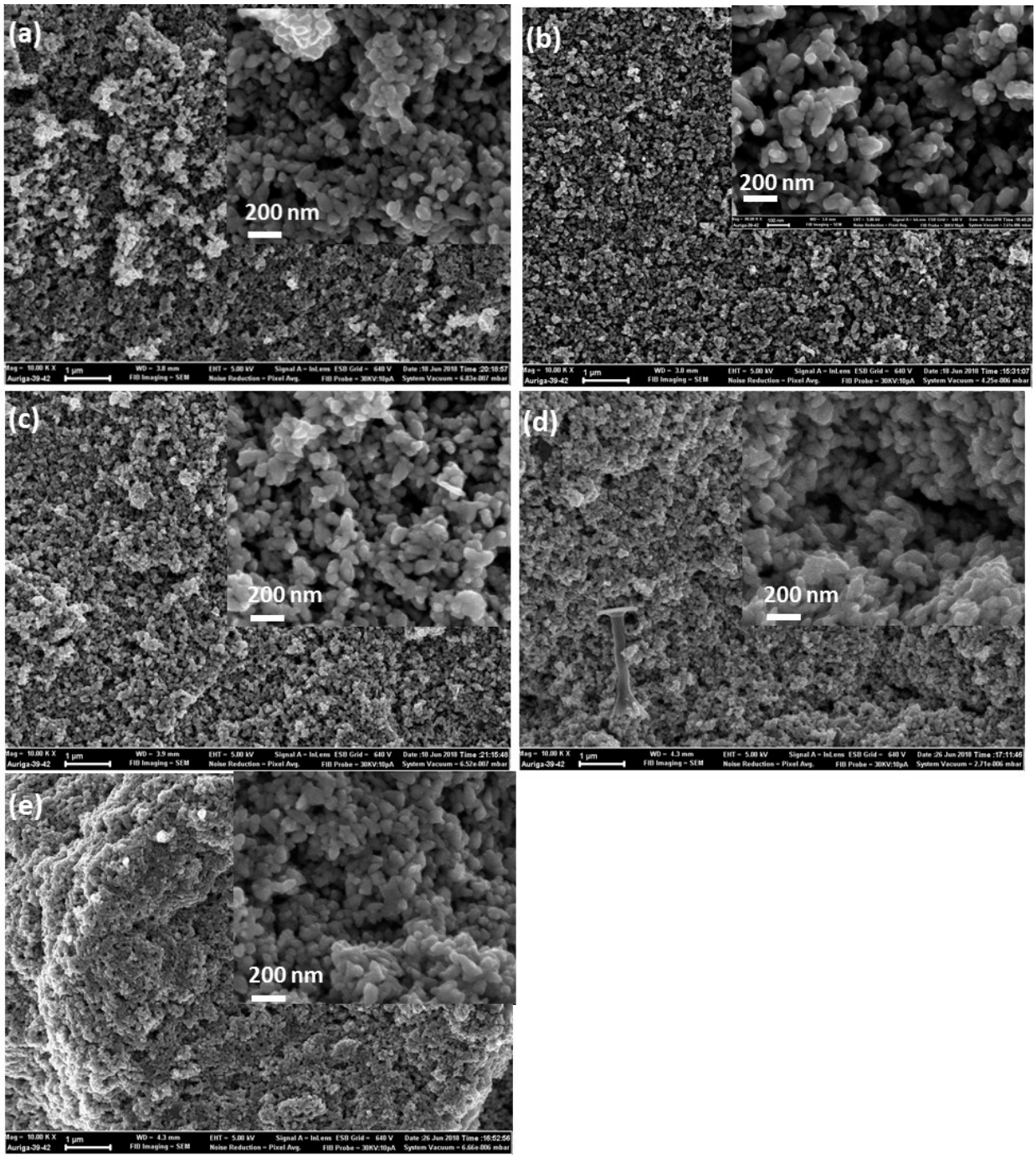

Figure 8. SEM micrographs of ZnO-8h@12.5pH after 60 min of treatment in the presence of (a) 10 mg/L SMX in UPW, (b) HA matrix, (c) 10 mg/L SMX in HA matrix, (d) SW matrix, and (e) 10 mg/L SMX in SW matrix.

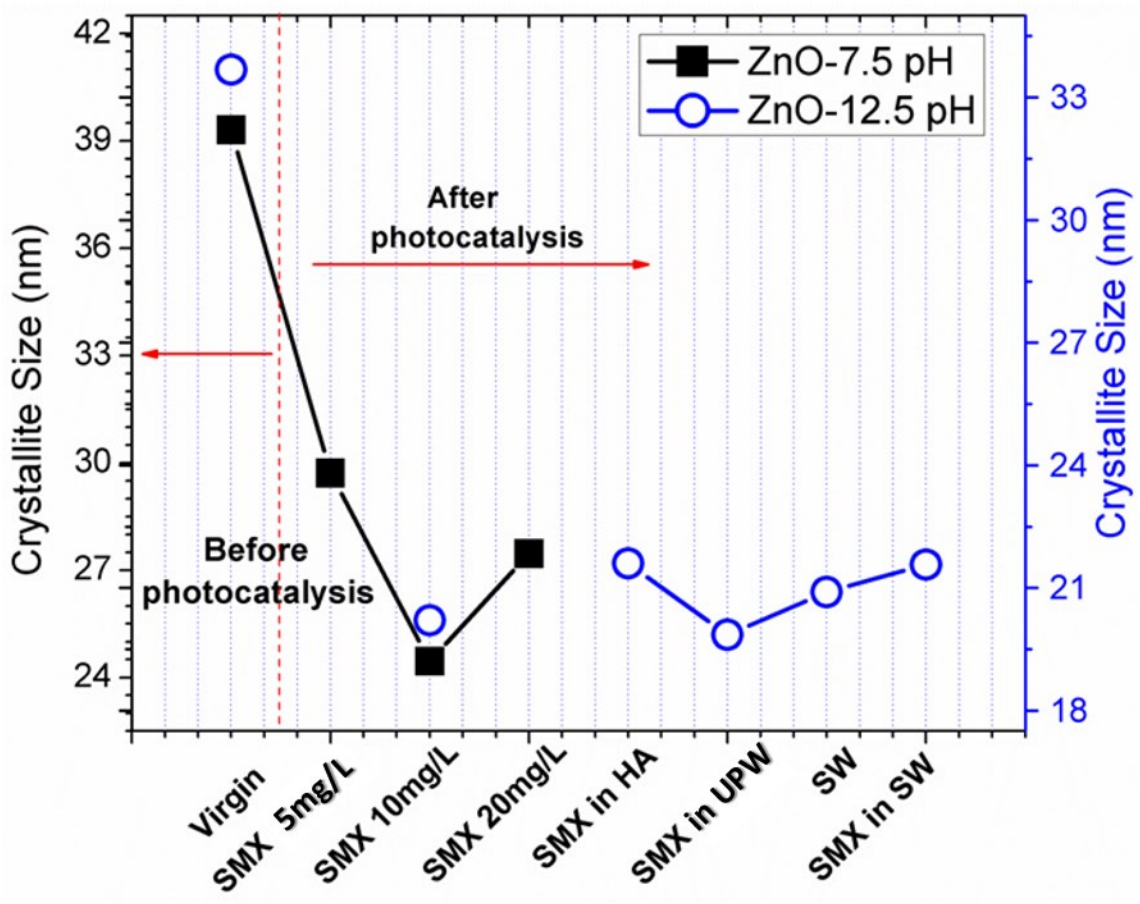

565

566 **Figure 9.** Evolution of the size of crystallites as a function of SMX initial concentrations and the

567 type of the water matrix.

568

569

570 **Supplementary Material**

571

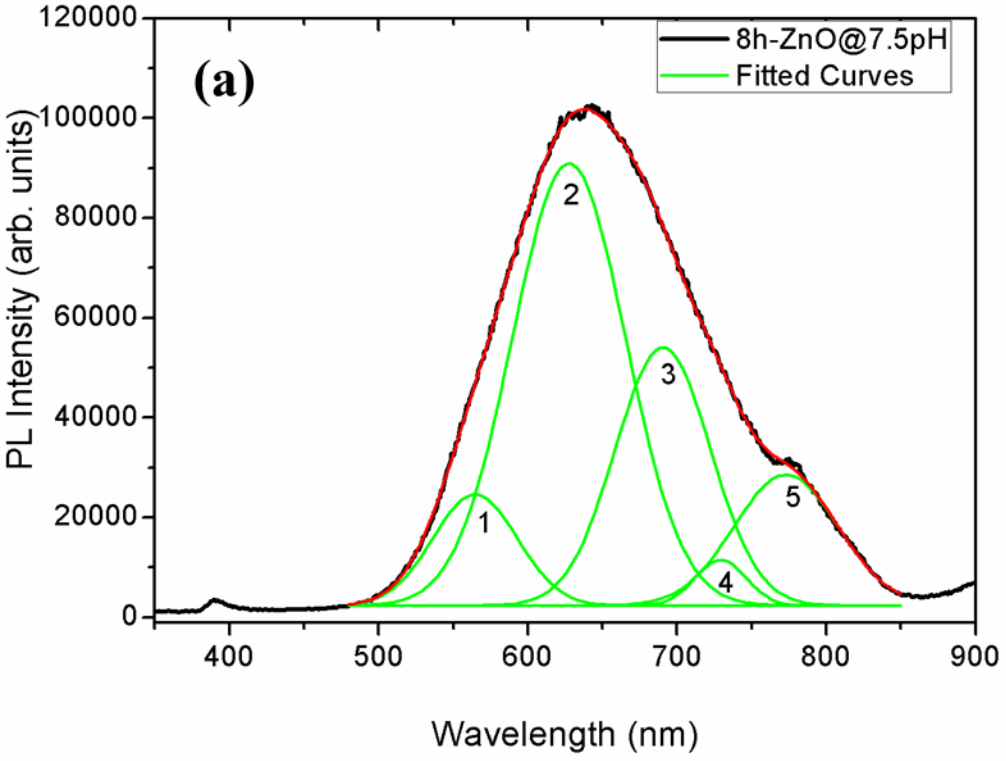

572

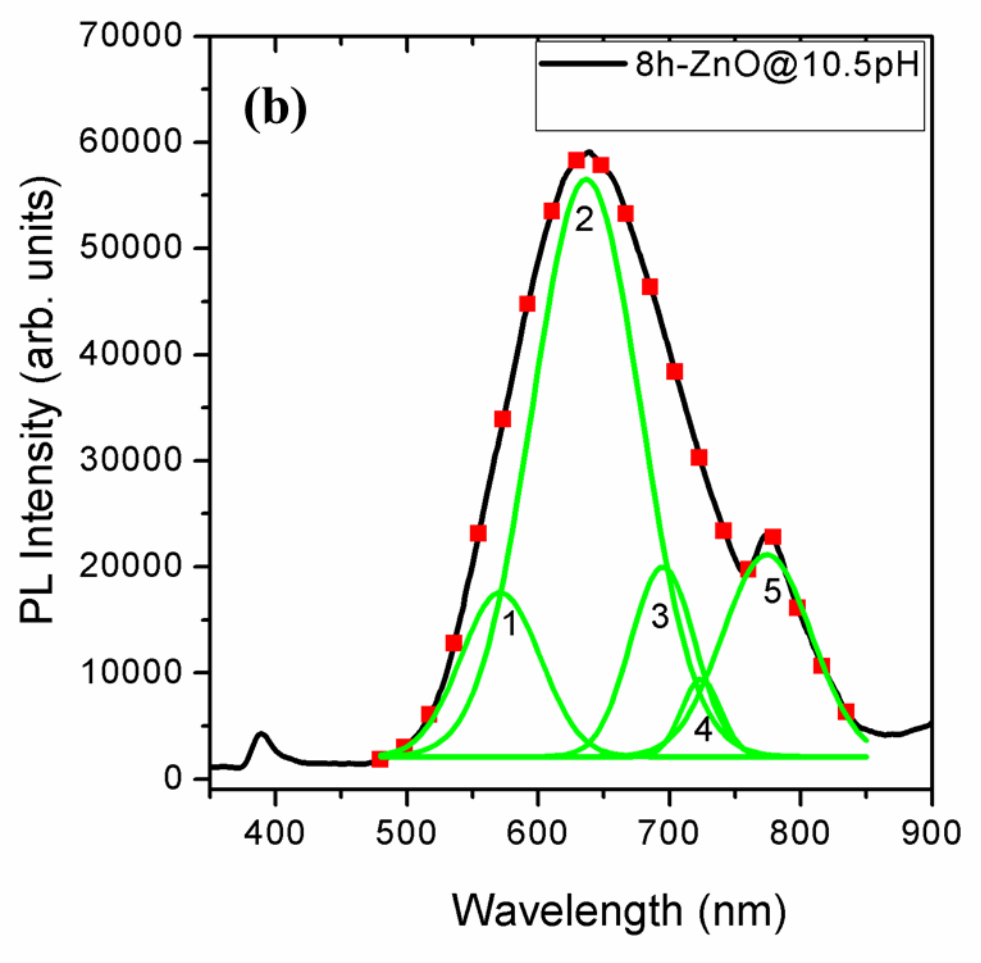
(b)
8h-ZnO@10.5pH
PL Intensity (arb. units)
Wavelength (nm)
70000
60000
50000
40000
30000
20000
10000
0
400
500
600
700
800
900
1
2
3
4
5

573

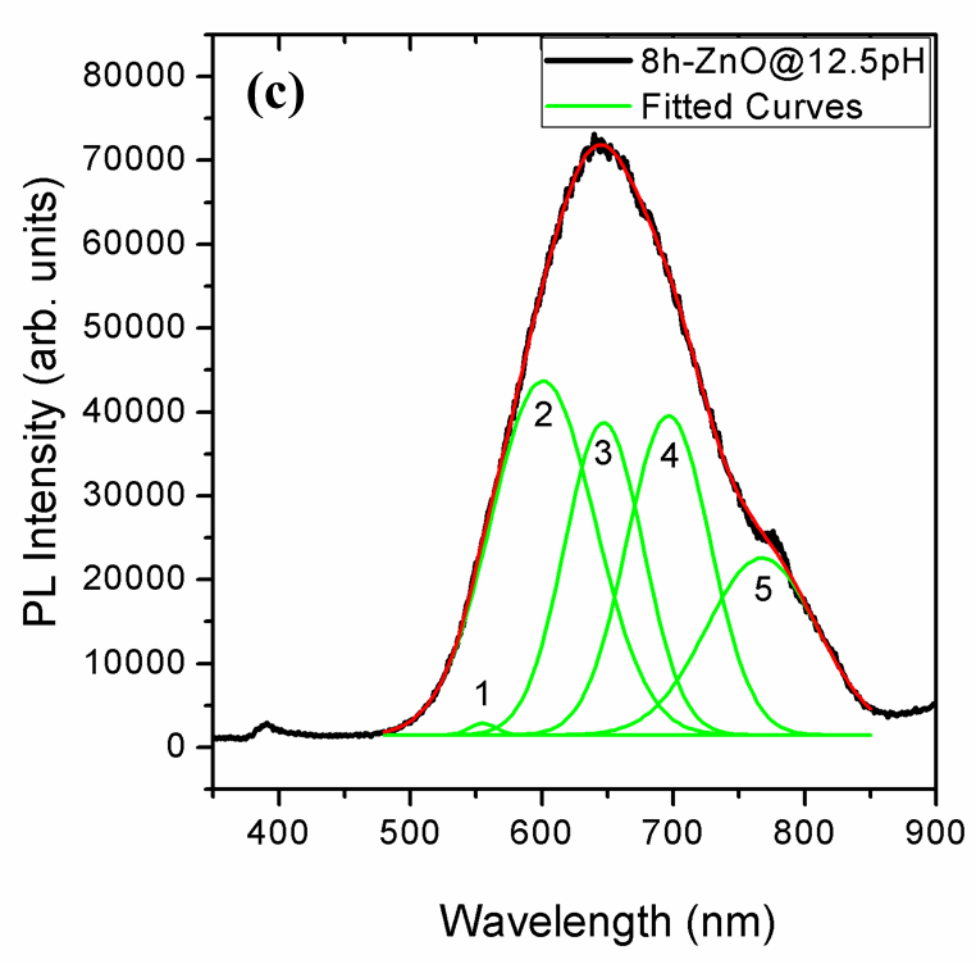

574

575 Figure S1. Photoluminescence (PL) spectra of the synthesized ZnO catalysts.

576